Обзор ArXiv/astro-ph, 29 марта – 4 апреля 2023

От Сильченко О.К.

83% -Массивные, быстро вращающиеся диски, но ТОЛСТЫЕ И ГОРЯЧИЕ

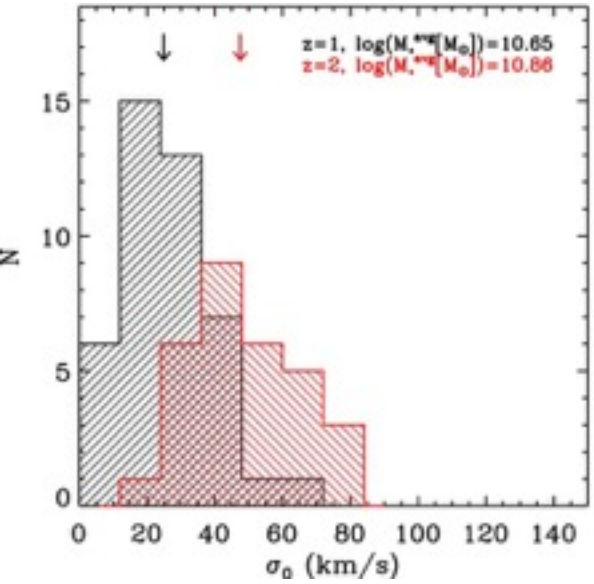

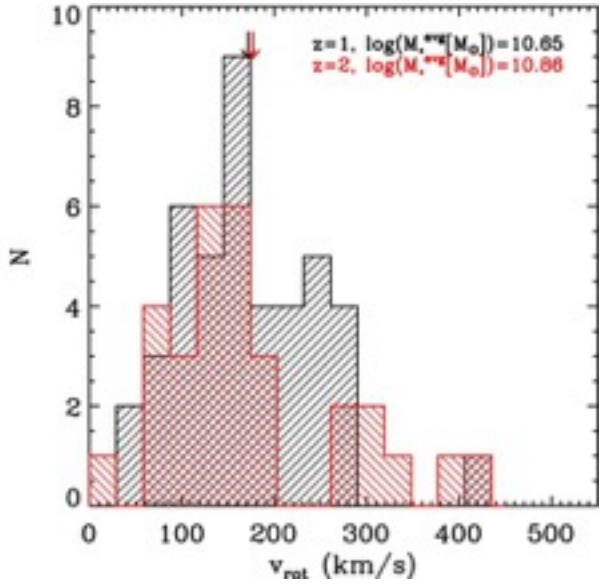

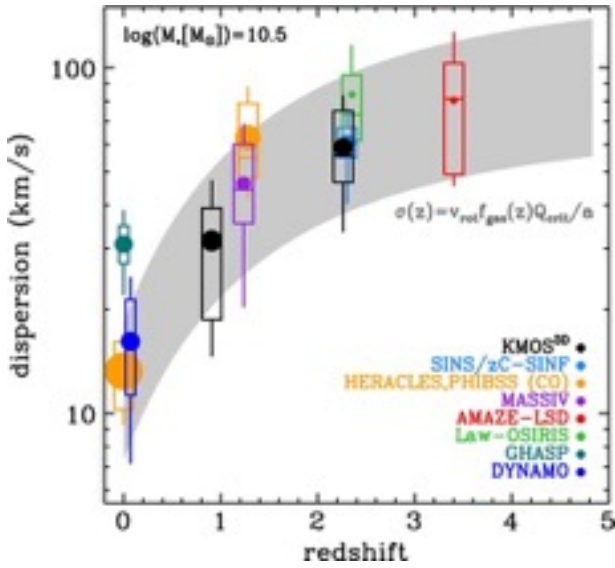

Wisnioski et al. 2015

Немонотонная эволюция турбулентных скоростей газовых дисков гигантских галактик

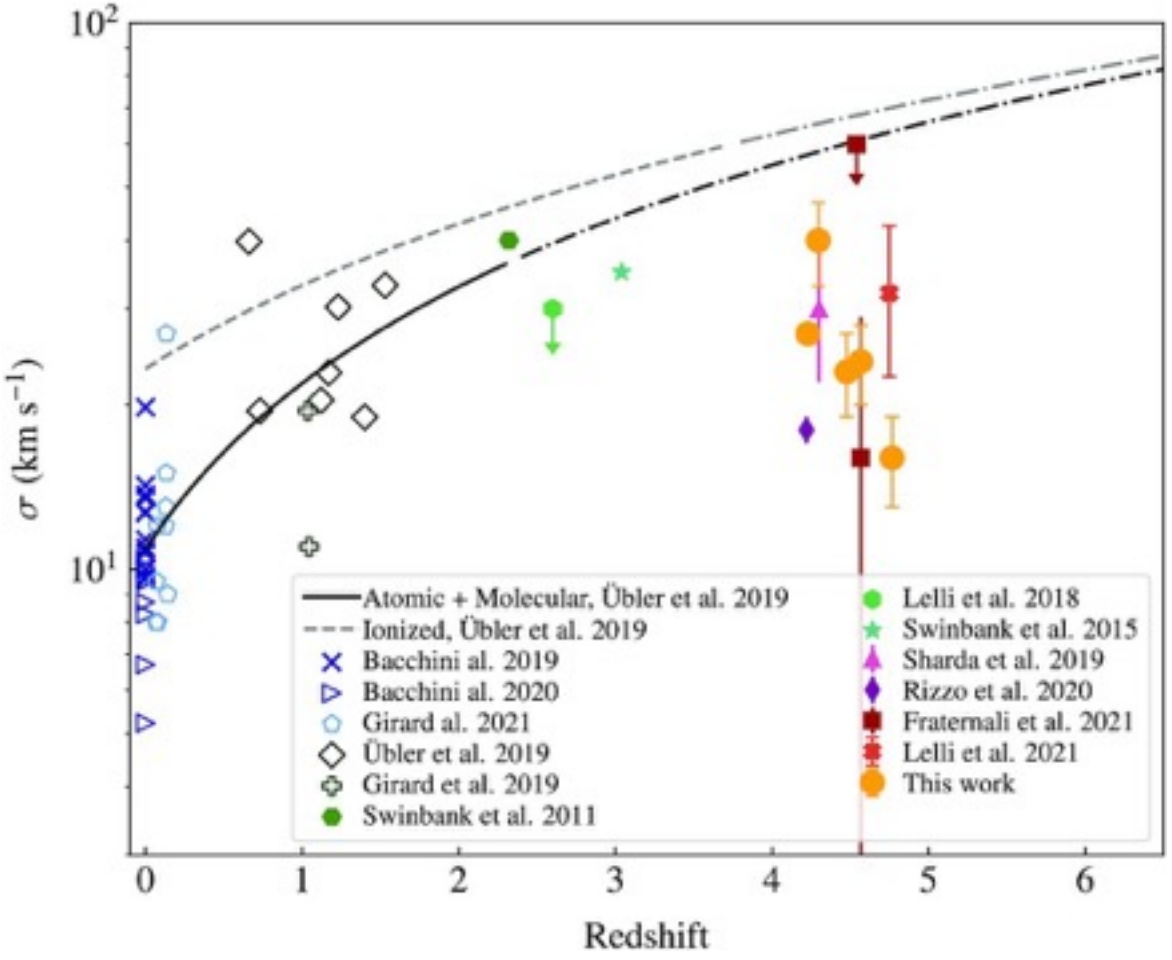

Rizzo+2020

ArXiv: 2303.16227

The ALMA-ALPAKA survey I

High-resolution CO and [CI] kinematics of star-forming galaxies at $z = 0.5$ - 3.5

F. Rizzo[1,2], F. Roman-Oliveira[3], F. Fraternali[3], D. Frickmann[1,2], F. M. Valentino[4,1], G. Brammer[1,2], A. Zanella[5], V. Kokorev[3], G. Popping[4], K. E. Whitaker[6,1], M. Kohandel[7], G. E. Magdis[1,8,2], L. Di Mascolo[9,10,11], R. Ikeda[12,13], S. Jin[1,8], and S. Toft[1,2]

[1] Cosmic Dawn Center (DAWN)
[2] Niels Bohr Institute, University of Copenhagen, Jagtvej 128, 2200 Copenhagen N, Denmark
e-mail: francesca.rizzo@nbi.ku.dk
[3] Kapteyn Astronomical Institute, University of Groningen, Landleven 12, 9747 AD, Groningen, The Netherlands
[4] European Southern Observatory, Karl-Schwarzschild-Str. 2, D-85748 Garching bei München, Germany
[5] Istituto Nazionale di Astrofisica, Vicolo dell'Osservatorio 5, 35122, Padova, Italy
[6] Department of Astronomy, University of Massachusetts, Amherst, MA 01003, USA
[7] Scuola Normale Superiore, Piazza dei Cavalieri 7, I-56126 Pisa, Italy
[8] DTU-Space, Technical University of Denmark, Elektrovej 327, DK-2800, Kgs. Lyngby, Denmark
[9] Astronomy Unit, Department of Physics, University of Trieste, via Tiepolo 11, Trieste 34131, Italy
[10] INAF – Osservatorio Astronomico di Trieste, via Tiepolo 11, Trieste 34131, Italy
[11] IFPU – Institute for Fundamental Physics of the Universe, Via Beirut 2, 34014 Trieste, Italy
[12] Department of Astronomy, School of Science, SOKENDAI (The Graduate University for Advanced Studies), 2-21-1 Osawa, Mitaka, Tokyo 181-8588, Japan
[13] National Astronomical Observatory of Japan, 2-21-1 Osawa, Mitaka, Tokyo 181-8588, Japan

Выборка

ID	Name	RA (deg)	Dec (deg)	redshift	Field/Survey	Notes
1	GOODS-S 15503	53.08205	-27.83995	0.561	GOODS-S	-
2	COSMOS 2989680	150.43186	2.80261	0.623	COSMOS	Minor merger
3	COSMOS 1648673	149.98144	2.25321	1.445	COSMOS	AGN(?)
4	ALMA.03	333.99393	-17.62988	1.453	XCS	Cluster member
5	ALMA.010	333.98853	-17.63149	1.453	XCS	Cluster member
6	ALMA.08	333.99266	-17.63950	1.456	XCS	Cluster member
7	ALMA.01	333.99233	-17.63737	1.466	XCS	Cluster member
8	ALMA.06	333.99880	-17.63306	1.467	XCS	Cluster member
9	ALMA.013	333.99909	-17.63797	1.471	XCS	Cluster member
10	SHiZELS-19	149.79817	2.39008	1.484	COSMOS	-
11	SpARCS J0225-371	36.44191	-3.92436	1.599	SpARCS	Cluster member
12	SpARCS J0224-159	36.11320	-3.40037	1.634	SpARCS	Cluster member
13	COSMOS 3182	150.07594	2.21182	2.103	COSMOS	Protocluster member
14	Q2343-BX610	356.53934	12.82202	2.211	SINS/zC-SINF	AGN(?)
15	GS30274	53.13114	-27.77319	2.225	GOODS-S	AGN
16	HXMM01-a	35.06938	-6.02830	2.311	HerMES	Group member
17	HXMM01-b+c	35.06907	-6.02904	2.308	HerMES	Group member, merger
18	HATLAS J084933-W	132.38994	2.24573	2.407	H-ATLAS	AGN, protocluster member
19	CLJ1001-131077	150.23728	2.33813	2.494	COSMOS	Cluster member
20	CLJ1001-130949	150.23691	2.33579	2.504	COSMOS	Cluster member
21	CLJ1001-130891	150.23986	2.33646	2.513	COSMOS	Cluster member
22	Gal3	150.33139	2.16239	2.935	COSMOS	-
23	ADF22.1	334.38507	0.29551	3.089	SSA2	AGN, protocluster member
24	ADF22.5	334.38416	0.29323	3.094	SSA2	Protocluster member
25	ADF22.7	334.38120	0.29946	3.088	SSA2	AGN, protocluster member
26	Gal5	149.87724	2.28388	3.339	COSMOS	-
27	Gal4	150.27827	2.25887	3.431	COSMOS	-
28	W0410-0913	62.54425	-9.21812	3.630	WISE	AGN, protocluster member

HST images + ALMA [CI],CO

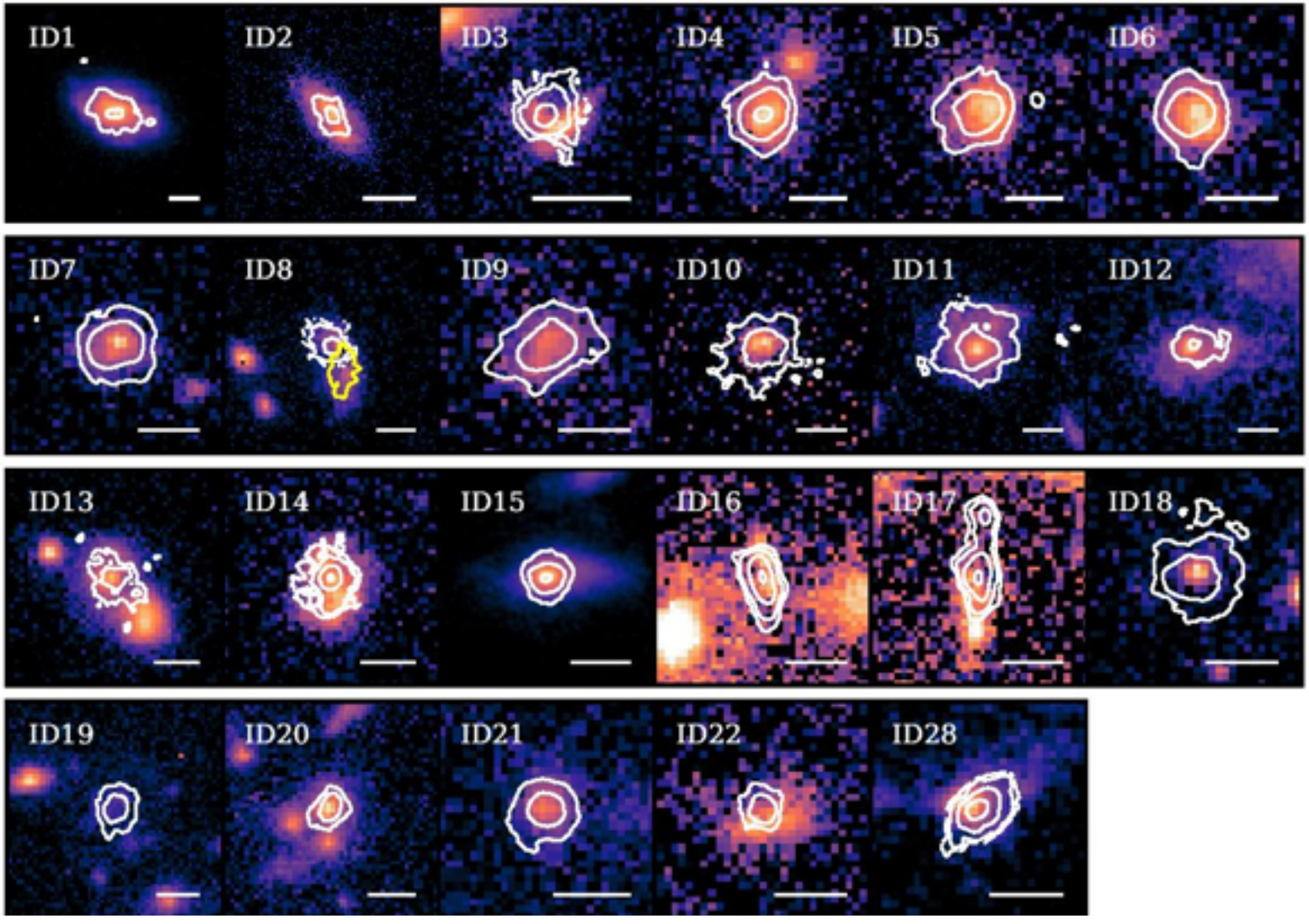

главная последовательность?, но на z>2.5 все starbursts

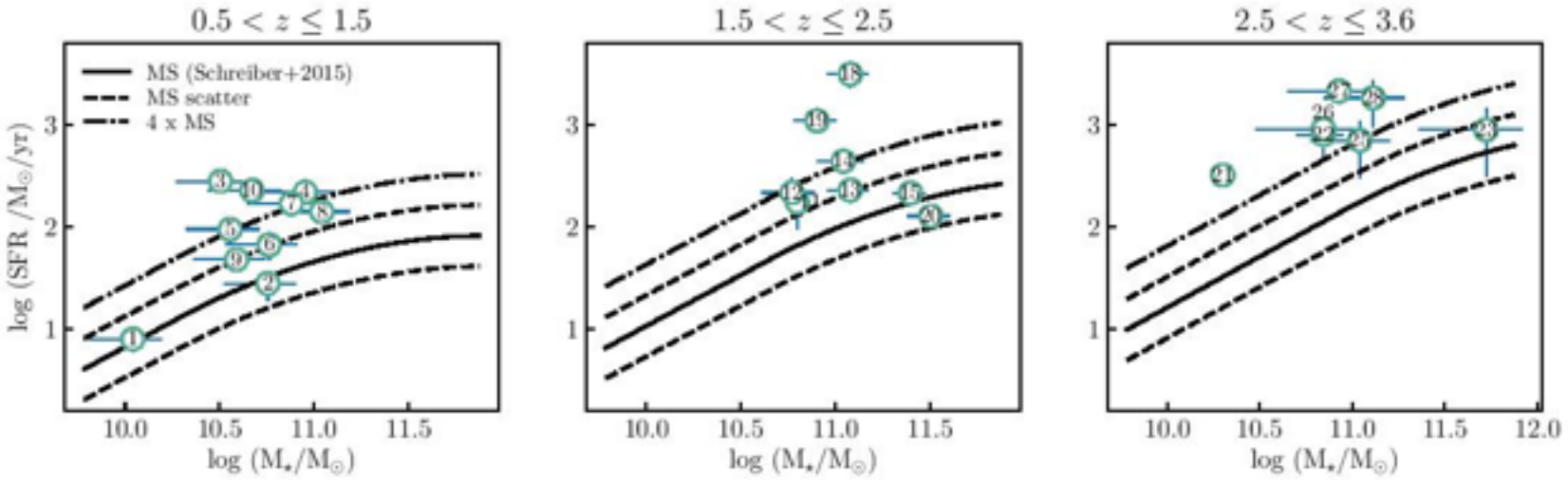

Fig. 3. Distribution of the ALPAKA galaxies in the stellar mass (M_*) - SFR plane, divided in three redshift bins. The solid line in the three panels show the empirical main-sequence relations from Schreiber et al. (2015) at z = 1.3, 2.2, 3, which are the average redshifts of ALPAKA targets in the three bins. The dashed and dot-dashed lines show the $\pm 1\sigma$ scatter and the line dividing the main-sequence and starburst galaxies, respectively (Rodighiero et al. 2011). We note that only the 25 ALPAKA targets with good estimates of both M_* and SFR are shown.

Круглые срелаксированные диски – звездные и газовые…

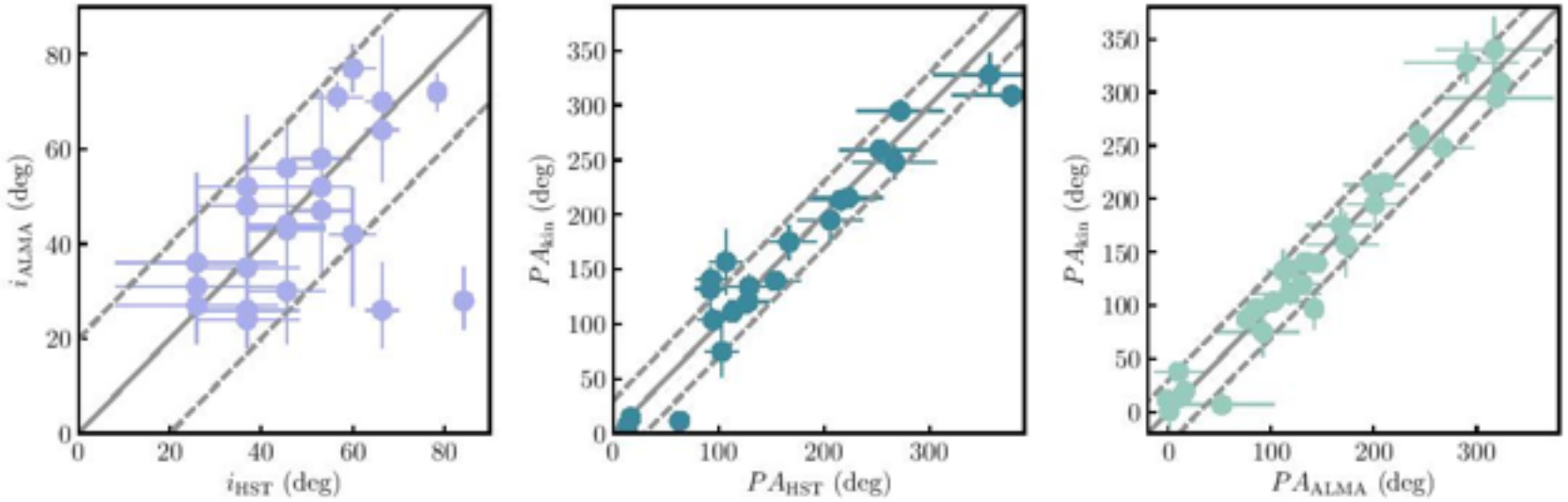

Fig. 5. *Left panel:* comparison between the inclination angles derived from the morphological fitting of HST and ALMA data using GALFIT and CANNUBI respectively. *Central panel:* comparison between the position angles derived from the morphological fitting of HST data with GALFIT and kinematic fitting of ALMA data with ^{3D}BAROLO. *Right panel:* comparison between the position angles derived from the morphological fitting of ALMA data with CANNUBI and the corresponding kinematic fitting. The gray line shows the 1:1 relation and the gray dotted lines show deviations at ±20 deg (left panel) and ±30 deg (central and right panels).

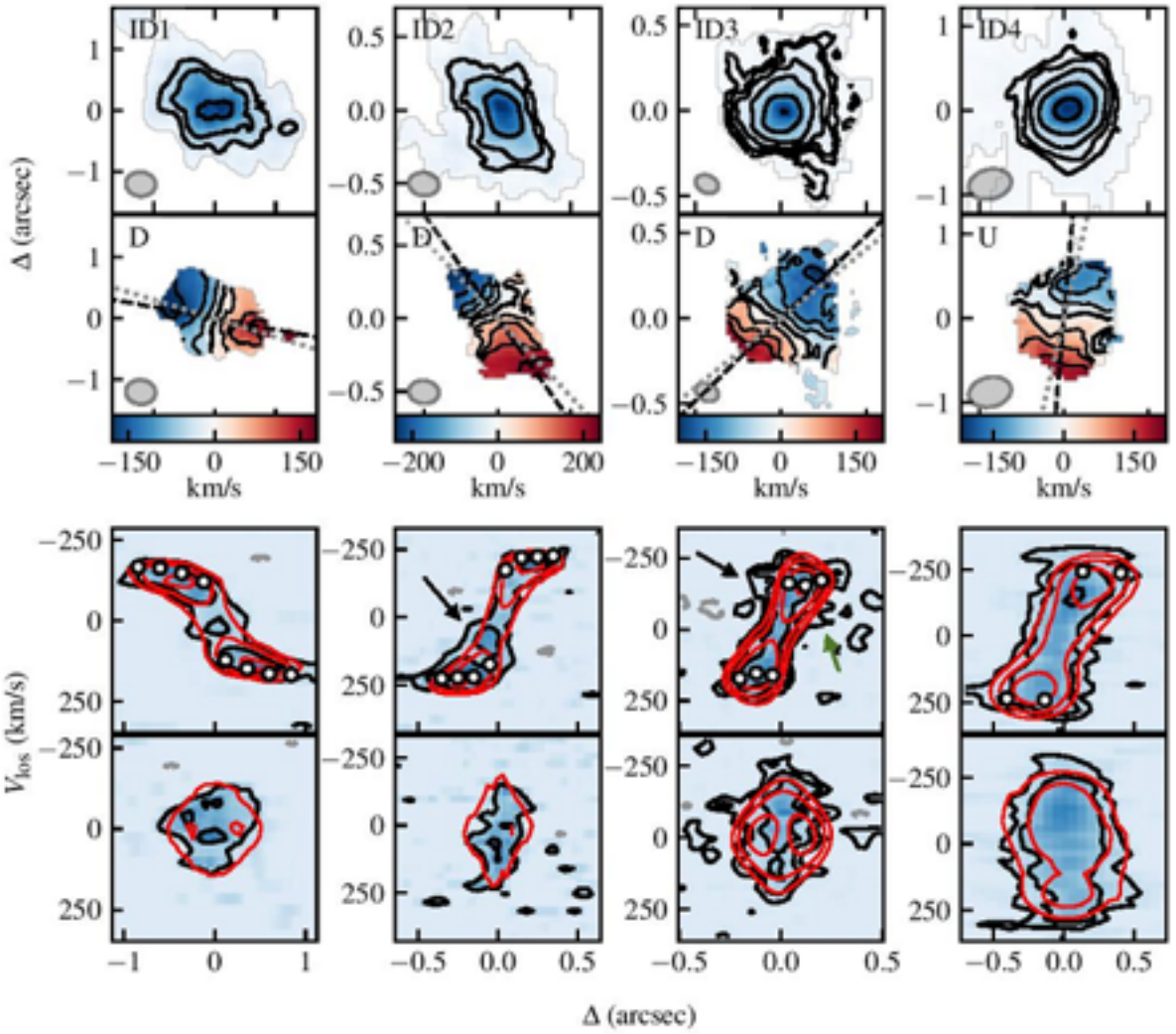

Fig. 6. For each target with ID in the upper left, we show from top to bottom: the total-flux map and the velocity field and the major and minor-axi PVDs. In the total-flux maps, the first external contour is a "pseudo-contour" (see Appendix B in (Roman-Oliveira et al. 2023) for details) at RMS. In the velocity field, the black lines show the iso-velocity contours, with the thickest one indicating the systemic velocity. The black dashe and gray dotted lines are the kinematic and morphological position angles, respectively. For the morphological position angle, we show the on obtained from fitting HST data when available and the total-flux map otherwise. The beam is shown in the bottom left. In the PVDs, the y-axi shows the line-of-sight velocities centred on the systemic velocity or redshift and the x-axis shows the distance with respect to the center of th kinematic model. The contours for the data (solid black) and the model (red) are at [1, 2, 4, 8, 16, 32] × 2.5 RMS. The gray dotted contours are a

Кривые вращения

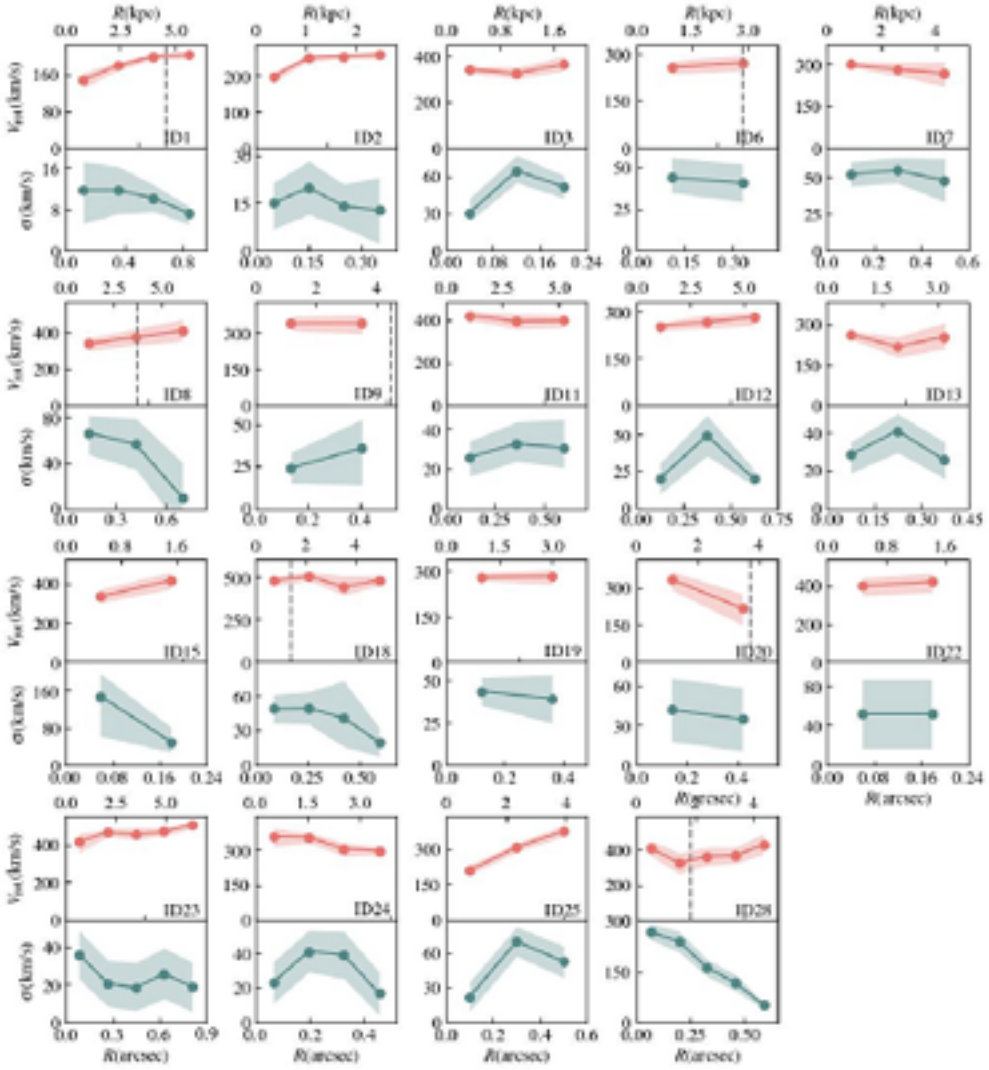

Главный результат – падение(?) дисперсии скоростей газа на z>3

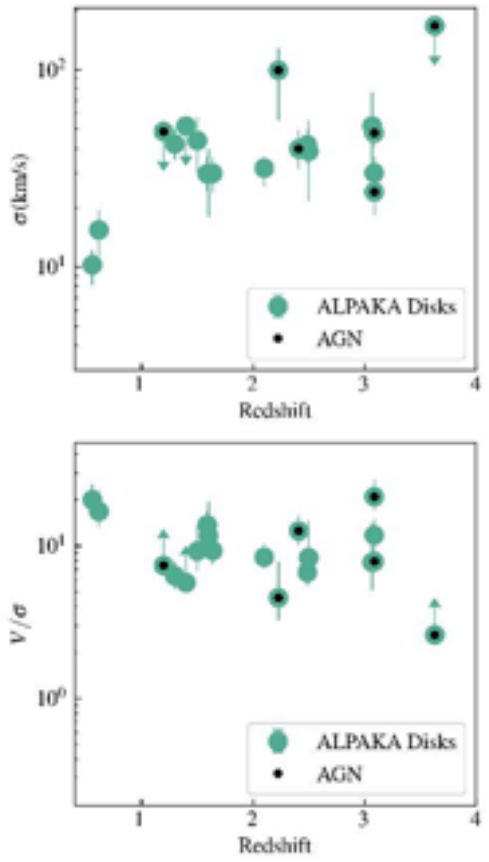

Fig. 9. Distribution of the ALPAKA disks in the velocity dispersion - redshift plane (upper panel) and rotation-to-velocity dispersion ratio - redshift plane (bottom panel). The values of σ_m and V_{max}/σ_m (Table 5.3) are plotted here. The redshifts of ID3, ID6 - 9, and ID19 are shifted by $|\Delta z| \leq 0.25$ for a better visualization of all the data points.

ArXiv: 2304.00036

ALMA hints at the presence of turbulent disk galaxies at $z > 5$

E. Parlanti[1], S. Carniani[1], A. Pallottini[1], M. Cignoni[2,3,4], G. Cresci[5], M. Kohandel[1], F. Mannucci[5], and A. Marconi[5,6]

[1] Scuola Normale Superiore, Piazza dei Cavalieri 7, I-56126 Pisa, Italy
[2] INAF – Osservatorio di Astrofisica e Scienza dello Spazio, Via Gobetti 93/3, 40129 Bologna, Italy
[3] Physics Departement, University of Pisa, Largo Bruno Pontecorvo, 3, 56127 Pisa, Italy
[4] INAF – Osservatorio Astronomico di Capodimonte, Via Moiariello 16, 80131, Napoli, Italy
[5] INAF – Osservatorio Astrofisico di Arcetri, Largo E. Fermi 5, 50127, Firenze, Italy
[6] Dipartimento di Fisica e Astronomia, Università di Firenze, Via G. Sansone 1, 50019, Sesto Fiorentino (Firenze), Italy

Received September 15, 1996; accepted March 16, 1997

ABSTRACT

Context. High-redshift galaxies are expected to be more turbulent than local galaxies because of their smaller size and higher star formation and thus stronger feedback from star formation, frequent mergers events, and gravitational instabilities. However, this scenario has recently been questioned by the observational evidence of a few galaxies at $z \sim 4-5$ with a gas velocity dispersion similar to what is observed in the local population.

Aims. Our goal is to determine whether galaxies in the first billion years of the Universe have already formed a dynamically cold rotating disk similar to the local counterparts.

Methods. We studied the gas kinematic of 22 main-sequence star-forming galaxies at $z > 5$ and determined their dynamical state by estimating the ratio of the rotational velocity and of the gas velocity dispersion. We mined the ALMA public archive and exploited the [C II] and [O III] observations to perform a kinematic analysis of the cold and warm gas of $z > 5$ main-sequence galaxies. We compared our results with what was found in the local and distant Universe and investigated the evolution of the gas velocity dispersion with redshift. We also compared the observations with theoretical expectations to assess the main driver of the gas turbulence at $z > 5$.

Results. The gas kinematics of the high-z galaxy population observed with ALMA is consistent within the errors with rotating but turbulent disks. We indeed infer a velocity dispersion that is systematically higher by 4-5 times than the local galaxy population and the $z \sim 5$ dust-obscured galaxies reported in the literature. The difference between our results and those reported at similar redshift can be ascribed to the systematic difference in the galaxy properties in the two samples: the disks of massive dusty galaxies are dynamically colder than the disks of dust-poor galaxies. The comparison with the theoretical predictions suggests that the main driver of the velocity dispersion in high-redshift galaxies is the gravitational energy that is released by the transport of mass within the disk. Finally, we stress that future deeper ALMA high-angular resolution observations are crucial to constrain the kinematic properties of

Выборка

Name	Line	Beam (arcsec)	Method	z	r_D (kpc)	inc (degree)	PA (degree)	$\log(\frac{M_{dyn}}{M_\odot})$	V_{max} (km/s)	σ_{gas} (km/s)	V_{max}/σ_{gas}
(1)	*(2)*	*(3)*	*(4)*	*(5)*	*(6)*	*(7)*	*(8)*	*(9)*	*(10)*	*(11)*	*(12)*
DLA0817g[b]	[C II]	0.21×0.15	I	4.249	$1.13^{+0.03}_{-0.03}$	41^{+5}_{-5}	108 ± 2	$10.8^{+0.2}_{-0.2}$	358^{+94}_{-74}	71^{+5}_{-5}	$5.04^{+1.81}_{-1.31}$
ALESS 073.1[b]	[C II]	0.17×0.14	I	4.746	$1.209^{+0.002}_{-0.002}$	32^{+3}_{-2}	45^{+1}_{-1}	$10.7^{+0.1}_{-0.1}$	324^{+91}_{-34}	54^{+1}_{-3}	$6.00^{+1.83}_{-0.91}$
HZ7	[C II]	0.35×0.32	I	5.245	$1.6^{+0.1}_{-0.1}$	< 47	269^{+29}_{-29}	$9.7^{+0.6}_{-0.7}$	81^{+83}_{-45}	85^{+12}_{-10}	$0.95^{+1.23}_{-0.58}$
HZ9	[C II]	0.30×0.25	II	5.529	$2.7^{+0.2}_{-0.2}$	...	...	10.8 ± 0.4	265^{+155}_{-97}	51^{+10}_{-9}	$5.19^{+4.80}_{-2.44}$
HZ4	[C II]	0.39×0.36	I	5.534	$2.07^{+0.04}_{-0.04}$	37^{+6}_{-10}	199^{+5}_{-6}	$10.0^{+0.2}_{-0.1}$	108^{+28}_{-12}	66^{+3}_{-3}	$1.64^{+0.52}_{-0.25}$
J1211	[C II]	0.80×0.57	I	6.019	$3.1^{+0.1}_{-0.1}$	45^{+16}_{-20}	272^{+16}_{-14}	$10.3^{+0.5}_{-0.3}$	149^{+116}_{-43}	58^{+9}_{-11}	$2.57^{+3.07}_{-1.01}$
	[O III]	0.76×0.57	I	6.029	$1.1^{+0.1}_{-0.1}$	44^{+22}_{-22}	293^{+26}_{-25}	$10.2^{+0.6}_{-0.5}$	155^{+160}_{-70}	54^{+18}_{-24}	$3.12^{+3.71}_{-1.27}$
J0235	[C II]	0.88×0.70	II	6.076	$1.8^{+0.4}_{-0.5}$	...	...	10.6 ± 0.3	219^{+107}_{-69}	72^{+101}_{-50}	$3.04^{+11.77}_{-2.16}$
	[O III]	0.69×0.63	II	6.090	$1.2^{+0.1}_{-0.1}$	...	...	10.6 ± 0.3	248^{+108}_{-75}	126^{+66}_{-53}	$1.96^{+2.90}_{-1.06}$
CLM1	[C II]	0.32×0.29	II	6.153	$0.9^{+0.1}_{-0.1}$	...	...	10.3 ± 0.3	195^{+92}_{-62}	42^{+16}_{-14}	$4.64^{+5.60}_{-2.34}$
J0217	[C II]	0.75×0.66	II	6.191	$4.1^{+0.8}_{-1.1}$	...	...	10.7 ± 0.3	136^{+63}_{-42}	> 83	< 1.63
	[O III]	0.68×0.56	I	6.203	$0.8^{+0.2}_{-0.1}$	< 60	80^{+59}_{-51}	< 10.4	< 227	111^{+27}_{-32}	< 2.8
VR7	[C II]	0.56×0.52	II	6.517	$2.3^{+0.1}_{-0.1}$	...	...	10.5 ± 0.3	189^{+79}_{-56}	57^{+15}_{-15}	$3.31^{+3.06}_{-1.46}$
UVISTA-Z-349	[C II]	1.65×1.17	I	6.564	$1.5^{+0.2}_{-0.2}$	36^{+26}_{-18}	238^{+55}_{-36}	$9.7^{+0.8}_{-1.0}$	81^{+128}_{-56}	77^{+13}_{-21}	$1.05^{+2.68}_{-0.77}$
UVISTA-Z-004	[C II]	1.36×1.15	II	6.669	$1.7^{+0.2}_{-0.2}$	...	...	10.4 ± 0.3	172^{+78}_{-54}	37^{+24}_{-19}	$4.64^{+9.24}_{-2.71}$
UVISTA-Z-049	[C II]	1.45×1.16	II	6.716	$1.0^{+0.1}_{-0.1}$	...	...	10.4 ± 0.3	208^{+94}_{-64}	51^{+46}_{-32}	$3.27^{+4.30}_{-1.83}$
UVISTA-Z-019	[C II]	1.39×1.21	II	6.740	$2.6^{+0.1}_{-0.1}$	...	...	10.5 ± 0.3	188^{+78}_{-55}	52^{+21}_{-17}	$3.61^{+3.98}_{-1.79}$
COS-29	[C II]	0.45×0.34	I	6.794	$1.5^{+0.2}_{-0.2}$	< 60	146^{+20}_{-33}	$9.5^{+0.6}_{-0.8}$	70^{+83}_{-44}	37^{+10}_{-13}	$1.89^{+4.48}_{-1.34}$
COS-30	[C II]	0.43×0.34	I	6.840	$1.3^{+0.3}_{-0.3}$	52^{+8}_{-9}	73 ± 5	$10.7^{+0.2}_{-0.1}$	264^{+36}_{-55}	68^{+14}_{-13}	$3.88^{+1.54}_{-1.33}$
	[O III]	0.89×0.60	II	6.851	$1.5^{+0.1}_{-0.1}$	...	...	10.2 ± 0.3	145^{+63}_{-44}	> 125	< 1.16
UVISTA-Z-001	[C II]	1.40×1.14	I	7.057	$1.3^{+0.3}_{-0.3}$	< 65	137^{+25}_{-32}	$10.5^{+0.6}_{-0.7}$	201^{+234}_{-116}	51^{+34}_{-32}	$3.94^{+18.95}_{-2.94}$
UVISTA-Y-004	[C II]	1.37×1.25	I	7.077	$1.7^{+0.2}_{-0.2}$	< 63	312^{+24}_{-19}	$10.1^{+0.7}_{-1.0}$	124^{+144}_{-85}	61^{+16}_{-30}	$2.03^{+6.61}_{-1.53}$
UVISTA-Y-003	[C II]	1.64×1.31	II	7.293	$1.6^{+0.1}_{-0.1}$	...	...	10.7 ± 0.3	281^{+120}_{-84}	63^{+25}_{-27}	$4.46^{+6.67}_{-2.16}$
UVISTA-Y-879	[C II]	1.44×1.25	I	7.357	$3.3^{+0.4}_{-0.4}$	< 65	143^{+22}_{-37}	$10.6^{+0.6}_{-1.2}$	212^{+215}_{-159}	119^{+36}_{-48}	$1.78^{+4.23}_{-1.44}$
SUPER8	[C II]	1.44×1.27	II	7.351	$2.2^{+0.4}_{-0.5}$	...	...	10.2 ± 0.3	134^{+61}_{-40}	74^{+100}_{-53}	$1.59^{+8.78}_{-1.22}$
UVISTA-Y-001	[C II]	1.57×1.28	I	7.660	$1.5^{+0.1}_{-0.1}$	< 60	122^{+31}_{-42}	$9.8^{+0.8}_{-0.9}$	90^{+139}_{-59}	79^{+11}_{-18}	$1.14^{+1.22}_{-0.79}$

Notes. *(1)* target name; *(2)* observed line; *(3)* beam FWHM; *(4)* best-fitting method; *(5)* redshift of the FIR line; *(6)* scale radius of the exponential disk; *(7)* disk inclination in degrees; *(8)* position angle of the galaxy; *(9)* logarithm of the dynamical mass in solar masses; *(10)* maximum rotational velocity as computed for an exponential disk with the dynamical mass and the scale radius obtained from the fitting; *(11)* best-fit velocity dispersion; *(12)* ratio of the maximum rotational velocity and the velocity dispersion.
[b] best-fit results with the model exponential disk + stellar bulge.

Сразу главный результат

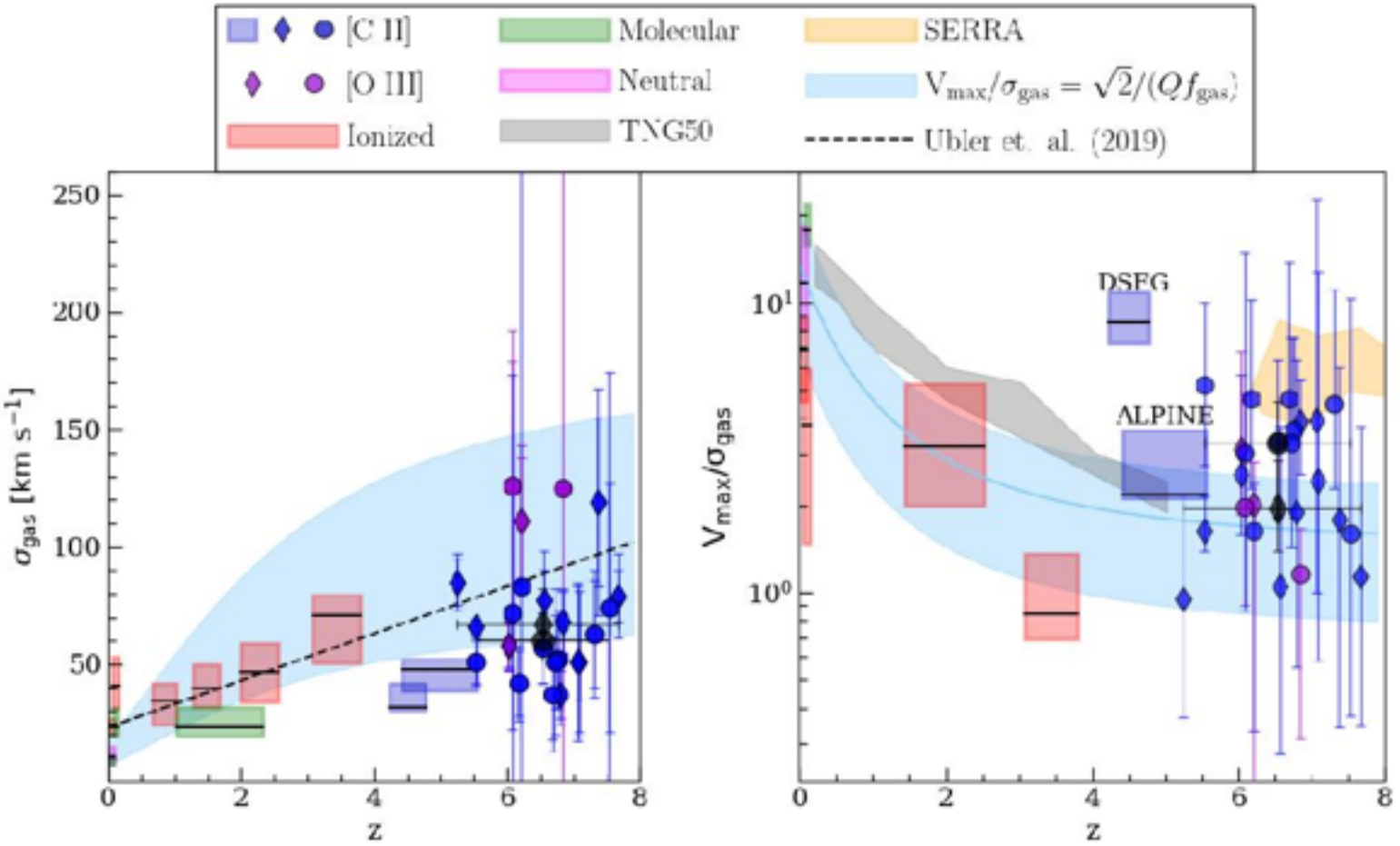

Все дело в режиме звездообразования?

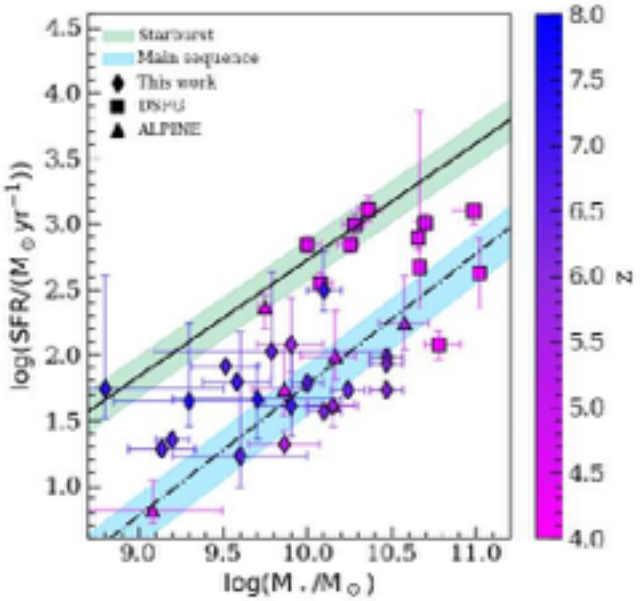

Fig. 5. SFR as a function of the stellar mass for our sample of galaxies and the results found in the literature. The colors represent the redshift on the galaxy (see the color bar). The diamonds are the galaxies targeted in this work. The squares show the results found by Sharda et al. (2019) Rizzo et al. (2020), Rizzo et al. (2021), Lelli et al. (2021) and Fraternali et al. (2021). The triangles show the ALPINE sample (Jones et al. 2021). In green we plot the starburst region at $z \sim 4 - 5$ as predicted by Caputi et al. (2017). In light blue we plot the main-sequence region

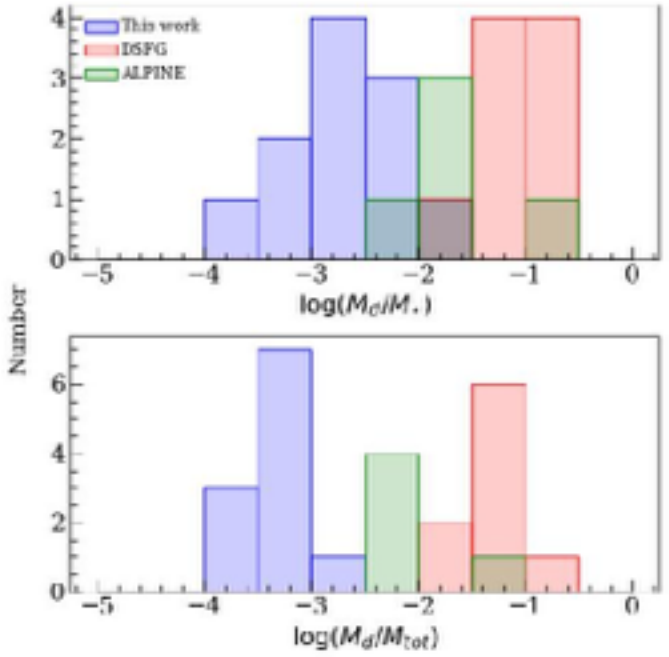

Fig. 6. Dust mass content in the three galaxy samples targeted in this work. In the upper panel, we plot the distribution of the ratio of the dust mass and stellar mass for the sample targeted in this work (in blue) and the sample of DSFG targeted by Rizzo et al. (2020, 2021), the starburst dusty galaxies (Sharda et al. 2019; Fratemali et al. 2021) (in red), and the ALPINE sample (Jones et al. 2021) (in green). In the lower panel we present the distribution of the ratio of the dust mass and total baryonic mass ($M_{gas} + M_*$) for the sample targeted in this work, the sample of

Или массы пыли?

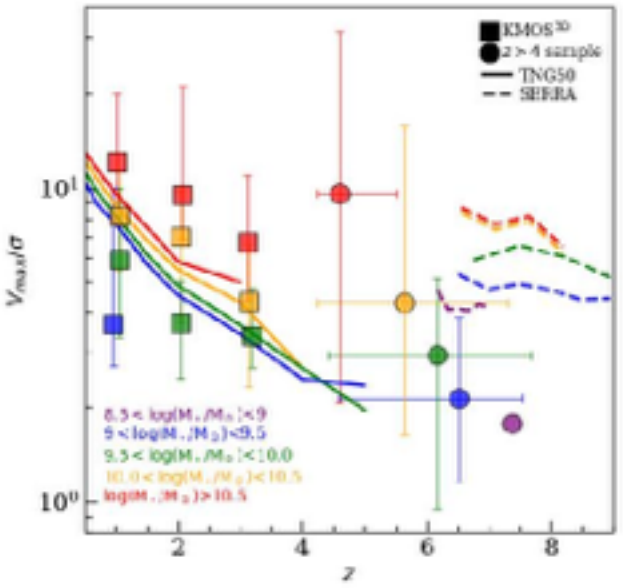

Fig. 7. V_{max}/σ_{gas} as a function of redshift and stellar mass. Squares represent the results from KMOS^{3D} (Wisnioski et al. 2019). Circles show the V_{max}/σ_{gas} for the whole $z > 4$ sample including the results of this work. Solid lines show the results obtained by TNG50 simulations (Pillepich et al. 2019). Dashed lines show the results obtained by SERRA simulations (Kohandel et. al. in prep). Different stellar mass bins are represented with different colors.

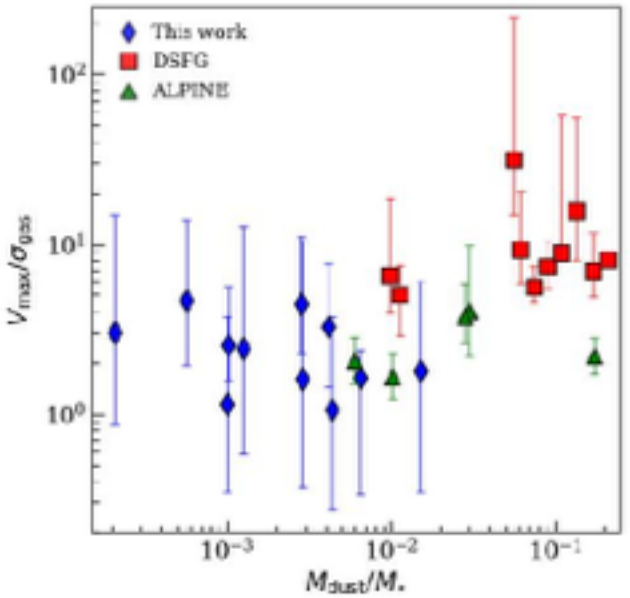

Fig. 8. V_{max}/σ_{gas} as a function of redshift, and the ratio of the dust mass and stellar mass. In red we show the DSFG sample (Sharda et al. 2019; Rizzo et al. 2020, 2021; Lelli et al. 2021; Fraternali et al. 2021), in green we plot the ALPINE sample (Jones et al. 2021), and in blue we show the sample targeted in this work.

and low-mass galaxies. Massive galaxies undergo fewer major mergers than less massive galaxies (Dekel et al. 2020), which

или доли газа в барионной массе?

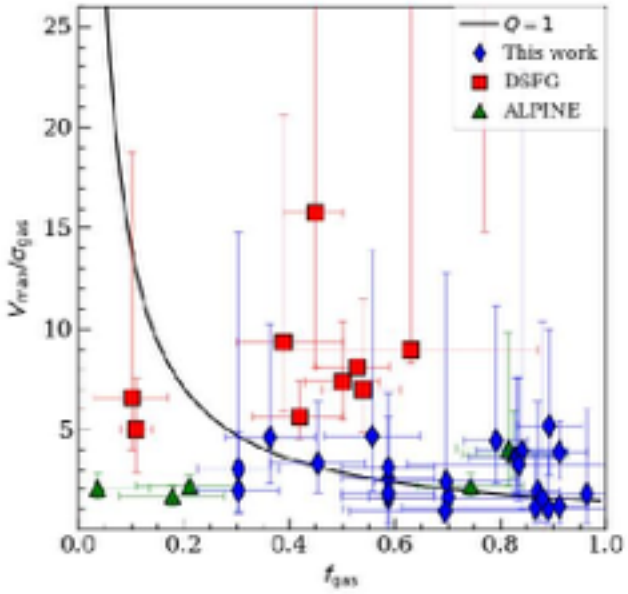

Fig. 9. V_{max}/σ_{gas} as a function of gas fraction. The black line represents the model by Wisnioski et al. (2015) with the assumption of Q=1 and a= $\sqrt{2}$. In dark blue, we show the data obtained from the sample of galaxies targeted in this work.

Все упирается в природу турбулентности газовых дисков

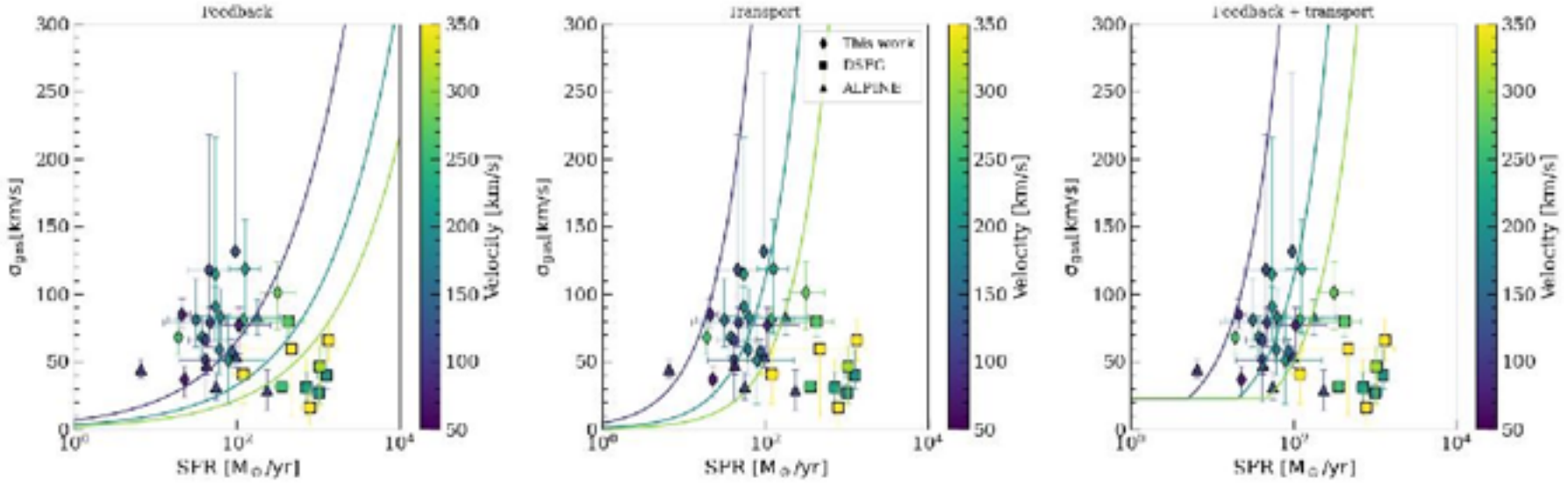

Fig. 10. Dependence of the velocity dispersion on the SFR and the rotational velocity. In the left panel, we show the model by Krumholz et al. (2018) with the feedback as the only driver of the velocity dispersion. In the central panel, we show the model with the release of gravitational energy due to the transport of the gas across the disk as the only driver of the velocity dispersion. In the right panel, we show the model with the combination of feedback and transport as drivers of the velocity dispersion.

Звездообразование= грав. неустойчивость

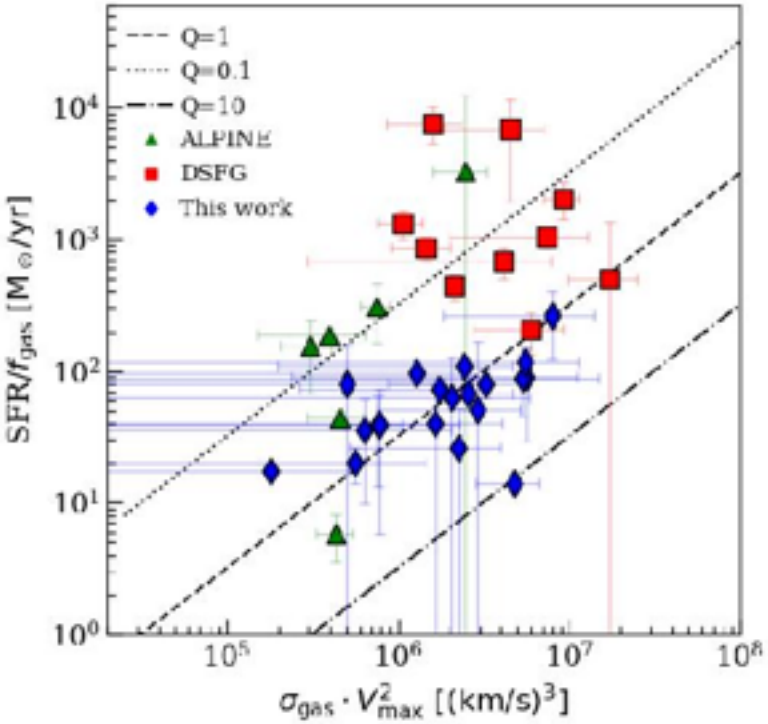

Fig. 11. Relation of the kinematical properties and SF-related properties for our sample of galaxies following Eq. 16. The dashed line corresponds to the model with $Q = 1$, the dotted line shows the model with $Q = 0.1$, and the dash-dotted line shows the model assuming $Q = 10$